NEUTRON SCATTERING IN MAGNETIC MATERIALS

R. Nathans and M. P. Schulhof

Some general aspects of the problem of neutron scattering (scattering law, instrumental resolution, etc.) as well as a number of special questions connected with the study of critical scattering in ferro- and antiferromagnetic systems are considered. New results of experiments on MnF_2 performed at the Brookhaven National Laboratory are discussed in terms of the susceptibility behavior near the critical temperature and from the view point of the dynamical scaling hypothesis

INTRODUCTION

In this paper we wish to discuss some experimental aspects of neutron scattering, and in particular magnetic scattering, especially in connection with work done at Brookhaven on critical scattering in ferro- and antiferromagnetic materials. We will be reviewing some well-known factors; in order to extract the the maximum amount of information from the data, they are worth going over. It is important for theorists to realize not only the great potential of neutron scattering methods but also their limitations.

Since critical effects require precise measurements, it is desirable to know just how far neutrons can be used to investigate the scattering law $S(q, \omega)$. Do experimental uncertainties arise solely from statistical errors? And, perhaps most important, how unique are our results?

To answer these and other questions, we first want to discuss the fundamentals of the method and then describe the recent experiments on critical scattering in MnF_2 made by Heller and ourselves [1].

The relationship between what can be measured experimentally and what can be theoretically learned is shown in Fig. 1. Experimentally, one determines the scattering intensity $I(q, \omega)$ as a function of the momentum transfer q and the energy transfer ω. This function is just the space-time Fourier transform of the correlation function (for the magnetization). Ideally it therefore enables us to obtain what is shown on the right of the figure – the correlation function as a function of space and time. But to obtain a complete description of the correlation function in space and time, one would have to measure $I(q, \omega)$ for all q and ω, where ω, the energy transfer, is equal to the difference between the initial and the final energies of the neutrons, and the wave vector $\mathbf{q}$ is related to the scattering vector $\mathbf{Q} = \mathbf{k}_0 - \mathbf{k}_\rho$ by the equation $\mathbf{Q} = 2\pi\boldsymbol{\tau} + \mathbf{q}$ (where $\boldsymbol{\tau}$ is a vector of the reciprocal lattice). To determine the behavior of spin-spin correlations at large distances and times, it is necessary to make measurements at small q and ω. On the other hand, if we are interested in short times and distances, we must make measurements at large q and ω. Thus, by controlling the q and ω region in the experiment, we can study the (r, t) region of the correlation function selectively.

Neutrons are very convenient for observing critical scattering since they enable one to make measurements at q and ω values that span several orders of magnitude. Of course, the region of possible q values is not infinite, any more than the range of ω values. The q and ω ranges characteristic of neutrons and light are compared in Fig. 2. For neutrons the values of q range from 0.01 to 10 $Å^{-1}$. For light this range is narrower and lower in value. However, laser interference methods mean that light can be used to study

State University of New York, USA; Brookhaven National Laboratory, USA. Published in Problemy Fiziki Élementarnykh Chastits i Atomnogo Yadra, Vol. 2, No. 4, pp. 1029-1046, 1972.

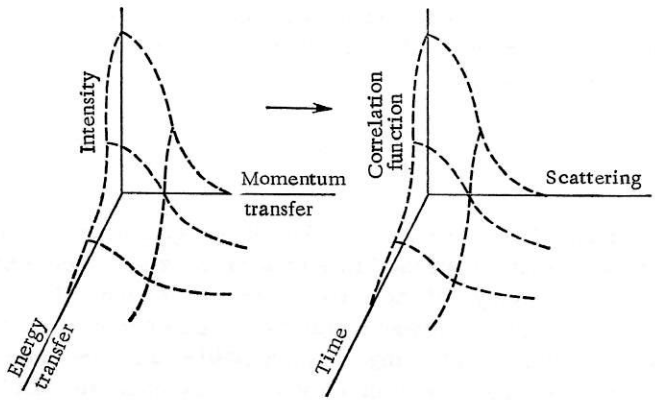

Fig. 1

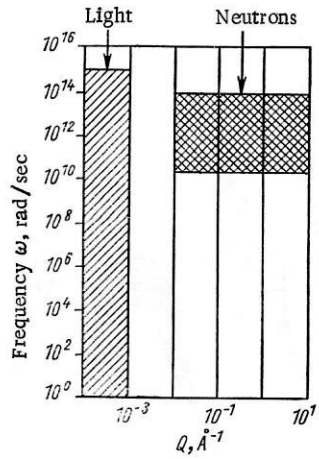

Fig. 2

Fig. 1. Relationship between the energy-momentum dependence of the scattering law S(q, ω) and the space-time behavior of the correlation function.

Fig. 2. Comparison between the ranges of the momentum transfer and energy transfer for neutron and light scattering.

processes in which the value of ω ranges from a few reciprocal seconds to as large a value as 10^{15} sec^{-1}. For neutrons the values of ω are restricted to the range 10^{10}–10^{14} sec^{-1} or, in electron volts, from 0.02 to 100 meV (for light from 10^{-12} to 1000 meV). Of course, the lower limits in q and ω for neutrons could be reduced by using neutrons with very long wavelengths, while the upper limit for light could be shifted upward by means of short-wavelength lasers; it then might be possible that the two methods would overlap. This would be particularly desirable for the study of fluctuation effects in liquids.

Let us consider the general expression for magnetic scattering of unpolarized neutrons by a system of N localized spins. The total differential cross section per unit solid angle and unit ω is

$$\frac{d^2\sigma}{d\Omega\, d\omega} = N\left(\frac{\gamma e^2}{mc^2}\right)^2 \frac{k_f}{k_i} |F(Q)|^2 \sum_{\alpha\beta}\left(\delta_{\alpha\beta} - \hat{k}_\alpha \hat{k}_\beta\right) S^{\alpha\beta}(q,\ \omega);$$

$$S^{\alpha\beta}(q,\ \omega) = \frac{1}{2\pi}\sum_r \int_{-\infty}^{\infty} \exp(iqr - i\omega t)\, \langle S_0^{\alpha}(0)\, S_r^{\beta}(t)\rangle\, dt.$$

Here k_f and k_i are the final and the initial momenta; F is the form factor associated with the spatial distribution of the magnetic electrons on which the neutrons are scattered; it is normalized to unity in the forward direction. The bracketed expression in the sum selects the components of S(q, ω) that are perpendicular to the scattering vector. Choosing directions of observations that correspond to particular reciprocal lattice vectors, we can separate the components of S(q, ω) perpendicular to the axis of easy magnetization from those parallel to this axis. The scattering law S(q, ω) is simply the Fourier transform of the spin-spin correlation function. For generalized critical diffuse scattering it can be represented in the form

$$S^{\alpha\beta}_{\text{diff}}(q,\ \omega) = \frac{kT}{g^2\mu_B{}^2}\ \chi^{\alpha\beta}(q)\left[\frac{\hbar\omega/kT}{1-\exp(-\hbar\omega/kT)}\right] F^{\alpha\beta}(q,\omega),$$

where χ, the susceptibility, depends on the wave vector, and F(q, ω), the spectral function, describes the decay of a plane wave of magnetization with time. The term in the square brackets symmetrizes the scattering for positive and negative values of ω.

Our tasks is to measure χ and F for magnetic systems of interest; χ depends only on the range of the correlations while F characterizes the dynamical behavior of the system. One can obtain a complete description of S(q, ω) in two ways: by measuring the total scattering, which gives all quantities simultane-

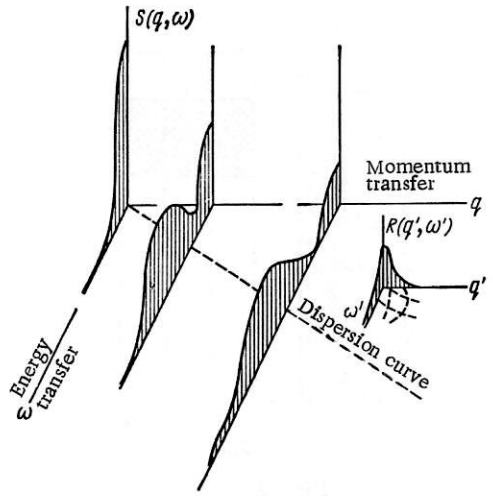

Fig. 3. Measurement of neutron scattering with allowance for finite resolution.

ously but with less accuracy; or by measuring the angular distribution, from which one determines $\chi(q)$ and then, using inelastic scattering, determine $F(q, \omega)$ with a higher degree of accuracy. In accordance with the fluctuation–dissipation theorem,

$$\int_{-\infty}^{\infty} \frac{1-\exp(-\hbar\omega/k_B T)}{\hbar\omega/k_B T} S_D^{\alpha\beta}(q, \omega)\, d\omega = \frac{k_B T}{g^2 \mu_B{}^2} \chi^{\alpha\beta}(q);$$

the integral over all frequencies of the symmetrized $S(q, \omega)$ can be simply expressed in terms of the static susceptibility. If the change of the wave vector due to inelastic scattering is small compared with the range of wave vectors over which the scattering is appreciable, then the angular differential cross section without energy analysis can be directly related to the susceptibility χ:

$$\left(\frac{d\sigma}{d\Omega}\right)_{\text{diff}} = \text{const} \sum_{\alpha\beta} (\delta_{\alpha\beta} - \hat{k}_\alpha \hat{k}_\beta) \frac{k_B T}{g^2 \mu_B{}^2} \chi^{\alpha\beta}(q).$$

This is the quasielastic approximation ($\hbar\omega / E_0 \ll 1$). This result is very useful for experimentalists; for it permits a simple two crystal experiment (without energy resolution) to determine χ with a relatively high statistical accuracy. This χ can then be used as input information in an analysis of the complete inelastic scattering measurements. The approximations this entails can be verified experimentally, and have been shown to be valid over a wide range of neutron energies.

Simple theoretical arguments show that χ should follow the Ornstein–Zernike law; that is, χ as a function of q is Lorentzian:

$$\chi(q) = \frac{A(T)}{\varkappa_1{}^2(T) + q^2}.$$

Here, the constant A depends weakly on the temperature; $\varkappa_1$, which is a reciprocal correlation length, depends on the temperature as a power, whose exponent varies from 1/2 in the molecular-field theory to 2/3 in the three-dimensional Ising model. Deviations from this behavior are expected near a phase transition and the modification proposed by Fisher allows for this by means of an η in the exponent:

$$\chi(q) = \left[\frac{A(T)}{\varkappa_1{}^2(T) + q^2}\right]^{1-\eta/2}.$$

It would be interesting to measure η and then compare its values with the theoretical predictions.

EXPERIMENTAL METHOD

The value of all experimental results may be of little or no significance if resolution effects are not allowed for properly in the interpretation of neutron measurements of $S(q, \omega)$.

To see how finite resolution can affect an experiment's results, let us represent the scattering as a function of the momentum transfer q along one axis and the energy transfer ω along another. Neutrons that are scattered into a detector have, because of the finite resolution, a spread of wave vectors, which arises from several factors. The neutron source is a reactor, in which the neutrons have a Maxwellian distribution and are emitted in all directions. Neutrons with a given energy must be extracted at a given angle from this distribution. But the collimators used to define the vector directions have a finite angular divergence. The monochromating crystal and analyzing crystal used to measure the initial and the final energy have a mosaic spread and therefore transmit a whole spectrum of momenta. In addition, the detector's sensitivity and the analyzer's reflectivity may introduce an asymmetric weighting function into the measured intensity. As a result, the measured intensity is a weighted sample of the scattering function surface about a certain nominal value.

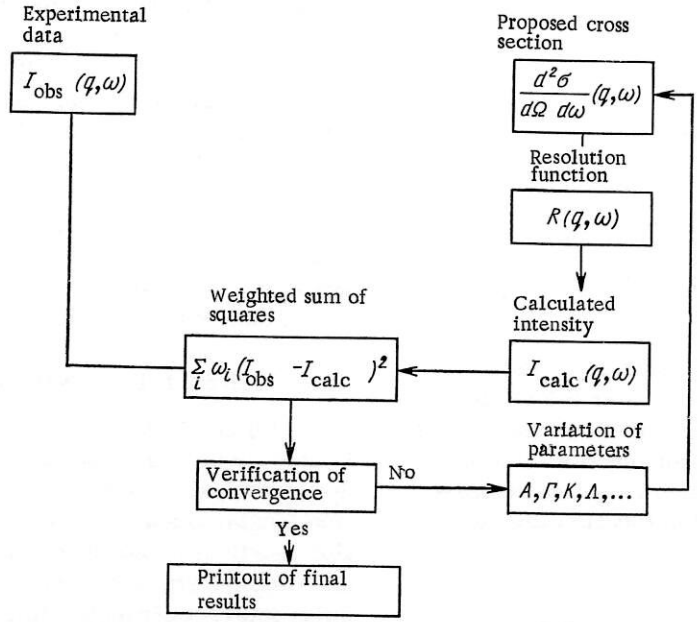

Fig. 4. Structural arrangement of the method of analyzing data.

We shall denote the instrumental resolution by $R(q', \omega')$ and regard it as a movable probe, whose amplitude is equal to unity for $q' = 0$ and $\omega' = 0$ and decreases in any direction in accordance with a Gaussian law. The analytic properties of this probe, which have been derived under certain simplifying assumptions by Cooper and Nathans [2], can be calculated directly if the instrumental parameters are known. The characteristics of the resolution function vary as one moves in the (q, ω) space, but what we observe is always a convolution of R and S. Thus, the intensity at certain value q_0 and ω_0 is the four-dimensional integral over $q'\omega'$ of the product of $R(q' - q_0, \omega' - \omega_0)$ and the scattering function S_0 (Fig. 3):

$$I(q_0, \omega_0) = \int_{q'} \int \int_{\omega'} \int R(q' - q_0, \omega' - \omega_0)\, S_0(q, \omega)\, dq'\, d\omega'.$$

Now suppose that $S(q, \omega)$ has a central diffuse peak (about $\omega = 0$) and lateral bands whose energy depends on q. Then there are three regions in which the resolution function is manifested in different ways. At large q and ω, the function $S(q, \omega)$ varies slowly, and the probe samples only one value. In this region the measured data accurately reflect the real cross section and no corrections are required. In the other limit – at small q and ω – the function $S(q, \omega)$ varies rapidly with respect to both variables, and the probe samples a large variation in the cross section. Thus, as we move the probe through succeedingly narrower regions, we can expect that our observations begin to characterize the resolution function rather than the intrinsic cross section. In the intermediate region, the situation is mixed and we must allow for the varying relationship between the resolution and the cross section in interpreting the data.

Since the majority of measurements correspond to the intermediate range we require a procedure for deconvolving the data from the resolution. Theoretically, this can be done in two ways. If information is gathered from a complete set of q, ω, inverse convolution is, in principle, possible. In practice, this is not feasible for a variety of reasons. Another way is to choose a reasonable form for the cross section, which includes unknown parameters, and determine the parameters by a fitting routine. This is the approach we have adopted.

The block form of the method we used to analyze the data is shown in Fig. 4. A theoretically reasonable form of the cross section $d^2\sigma/d\Omega d\omega$ is chosen with initial values taken for the free parameters. This cross section is then convoluted with the analytic resolution function R, which has been experimentally verified to describe the true resolution function for the particular set of instrumental constants employed. The calculated intensity is then compared with the experimental data, where factors like the background and incoherent scattering are already subtracted off. The usual weights (weighted sum of squares) are de-

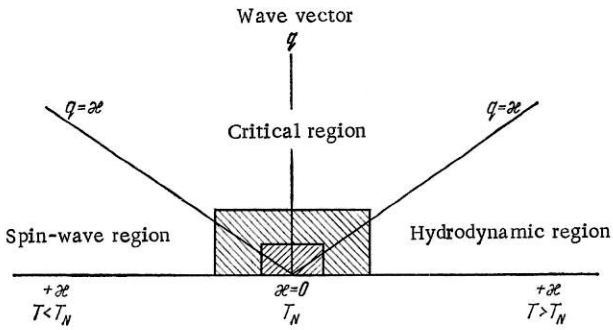

Fig. 5. Ranges of q and $\varkappa$ values that characterize the magnetic susceptibility near the critical temperature: the inner hatching shows the region inaccessible to neutron measurements. The outer hatched region is that in which large corrections associated with the resolution function are required.

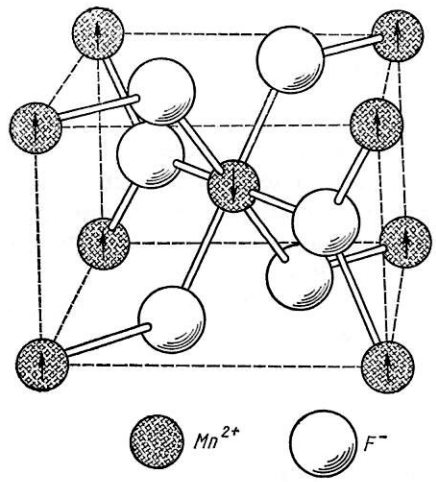

Fig. 6. Structure of the uniaxial antiferromagnet MnF_2.

termined from the counting statistics. The parameters extracted in this least-squares method could, for example, be the spin diffusion constant, the correlation length of the spin interactions, the overall normalization, relaxation times, etc. This procedure has the usual shortcomings of all methods of matching parameters. One has problems with convergence, the mesh size for the numeric integration, and the uniqueness of the results. Nevertheless, when all available information has to be exploited, such methods of data analysis must be employed.

RESULTS AND DISCUSSION

Figure 5 shows the region near the critical temperature, which can be characterized by two independent parameters: $\varkappa$, the reciprocal correlation length, and q, the wave number. The correlation length is a property of the scattering system and characterizes the distance within which the spins interact strongly. This length tends to infinity when T reaches T_N and, accordingly, $\varkappa$ tends to zero. The wave number, q, describes the size of the region in which a given characteristic of the spin dynamics is manifested, i.e., q and $\varkappa$ are the variables that determine the critical behavior.

The lines $q = \varkappa$ are the boundaries described by Halpern and Hohenberg [3]. Above T_N and for q less than $\varkappa$ hydrodynamics is applicable. One expects the relaxation rates to be spread about an individual peak concentrated near $\omega = 0$. The region below T_N with q less than $\varkappa$ is the region of spin waves; here one should observe waves for transverse fluctuations and diffusive modes for fluctuations parallel to the spin axes. Near the phase transition all the q become larger than $\varkappa$, and we arrive in the critical region, with spin properties in a transitional state.

Note that far from the critical point (with respect to q or $\varkappa$) the scattering function $S(q, \omega)$ varies slowly and resolution effects can be ignored. However, in this region, which is shown in Fig. 5 by the white unhatched space, the susceptibility is low and the statistical indeterminacy of the results is greater.

If we approach T_N for small wave numbers (the outer hatched region) the scattering peak becomes sharper, and its intensity increases. The majority of neutron data are obtained here, and the resolution problems for them is fairly acute. For internal consistency it is always necessary that the cross section proposed for one region should go over smoothly into that for another region wherever the cross sections overlap. The inner hatched region illustrates that area not accessible to neutrons since the cross sections vary much more rapidly than the measuring probe. This means that extreme temperature control is not necessary in neutron measurements because the resolution difficulties prevent us working very near T_N.

The theory of dynamical scaling makes several predictions concerning the characteristic frequency in each of these regions. One of our primary interests was to verify these predictions. The first extensive measurements of the behavior of the scattering law $S(q, \omega)$ for dynamic and static responses were made by Lau et al. [4] for the simple cubic lattice of $RbMnF_3$. The next logical step was to consider anisotropic systems, of which the simplest is MnF_2—a uniaxial antiferromagnet which orders at 67.5°K. We decided to make comprehensive measurements of $S(q, \omega)$ both above and below the transition, because this is a case where longitudinal and transverse fluctuations can be studied separately and one can measure $X_{\parallel}$ and

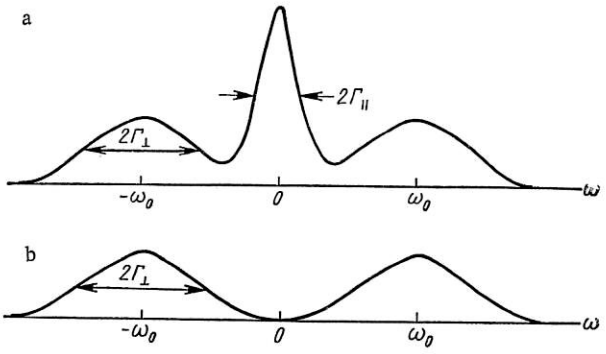

Fig. 7. Assumed differential cross sections for scattering by longitudinal and transverse spin fluctuations in MnF_2 near the critical temperature: a) $(d^2\sigma^{\parallel}/d\Omega d\omega) + \frac{1}{2}(d^2\sigma^{\perp}/d\Omega d\omega)$; $(d^2\sigma^{\parallel}/d\Omega d\omega) \sim (1/\varkappa_{\parallel}^2 + q^2) \cdot (\Gamma_{\parallel}/\Gamma_{\parallel}^2 + \omega^2)$; b) $(d^2\sigma^{\perp}/d\Omega d\omega) \sim (1/k_{\perp}^2 + q^2)\{\Gamma_{\perp}/[\Gamma_{\perp}^2 + (\omega - \omega_0)^2] + \Gamma_{\perp}/[\Gamma_{\perp}^2 + (\omega + \omega_0)^2]\}$.

$X_{\perp}$ as functions of the temperature. Since Heller's nuclear magnetic resonance data were also available for this system, we could compare the two methods. We also had the possibility of verifying the theory of dynamic scaling more fully.

Figure 6 shows that MnF_2 has a rutile structure with manganese atoms sitting at the corner sites (one spin direction) and in the center of the system (oppositely directed spin in the ordered state). Because of this magnetic structure one can study purely magnetic scattering without interference from Bragg peaks or acoustical phonons. Further, observing two reflections at angles that differ by 90°, one can separate the effects of scattering by longitudinal and transverse spin fluctuations, something that would be impossible in a cubic system with random domain structure. This means we can map out $S(q, \omega)$ separately for longitudinal and transverse fluctuations.

The proposed form of the scattering cross section is shown in Fig. 7. For the parallel direction (Fig. 7a) we observe the sum of three peaks: a central diffuse peak with width Γ, the result of longitudinal fluctuations, and two lateral peaks due to the transverse components. These sidebands can be measured directly from the 001 reflection, as is shown in Fig. 7b. Here, it is again assumed that the curves have a Lorentzian profile centered about $\pm\omega_0$. Below T_N they become spin waves. The transverse relaxation rates are fitted separately, the transverse $\varkappa$ being taken from experiments with two crystals. The fitting procedure has an advantage in that one can obtain the longitudinal and transverse components of the fluctuations both above and below T_N. The good quality of the fitting procedure is illustrated in Fig. 8. This figure shows data from a mixed reflection covering three temperature ranges: below, at, and above T_N. The continuous curves through the experimental points are the computer-calculated fit to Lorentzian curves folded with the resolution function. The transverse parameters had already been found and fixed for this set of data. The excellent agreement was obtained with only a single instrumental constant! The measurements were made for q values from the center of the Brillouin zone to 0.4 of the zone boundary. This covers the region in which scattering is most appreciable. The agreement between the experimental data and the theory with allowance for resolution gives confidence in this procedure for analysis.

We now pose the question: how does the longitudinal relaxation rate vary as a function of the temperature and wave vector? The answer to this question is shown in Fig. 9. Below T_N the widths are small and vary slowly with the temperature. There is a substantial increase near the transition, and then, except for small values of q, the widths again vary slowly with the temperature above T_N. At $q = 0$ the temperature dependence is almost linear, and the width tends to zero as T approaches T_N from above. Below T_N, the $q = 0$ width agrees with a zero width or at least with a width much less than the resolution. The presence of magnetic Bragg peaks below T_N makes it impossible to carry out accurate measurements at $q = 0$, although one can estimate the width by extrapolating the data from the region of small q. One of the interesting features of these results is the behavior of the widths below T_N. If there is symmetry about the critical point, the widths should again increase for small q.

Various aspects of the dynamical scaling hypothesis can be verified on the basis of these data. Measuring the $q = 0$ widths above the phase transition as a function of $\varkappa$ and the widths as a function of q at $T = T_N$, we find a power-law behavior with the same powers. For an isotropic system the power should be 3/2, as was found in $RbMnF_3$. It is not known precisely what power an anisotropic system should have. Figure 10 gives the answer to this question. Later we shall also discuss the possibility of applying a single universal scaling function to all our results. This function, if it exists, must not depend on q and $\varkappa$ separately, but only on the ratio $q/\varkappa$, where $\varkappa$ is the reciprocal correlation length. In Fig. 10 the longitudinal and transverse relaxation rates are plotted as a function of $\varkappa^{3/2}$ on the left. It is interesting to note that both components are linear functions of this quantity. As the anisotropy would lead one to expect, the transverse component does not tend to zero as $T \to T_N$. The fitted values of the exponents are 1.49 and 1.48.

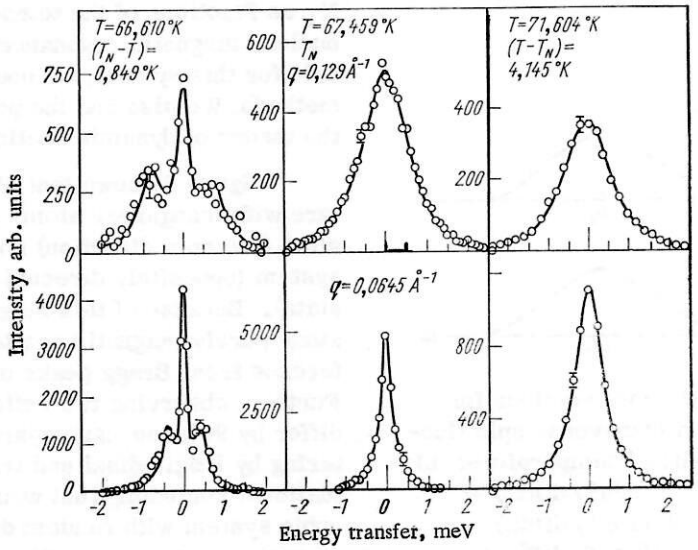

Fig. 8. Experimental results of neutron scattering by the antiferromagnet MnF_2 near the critical point.

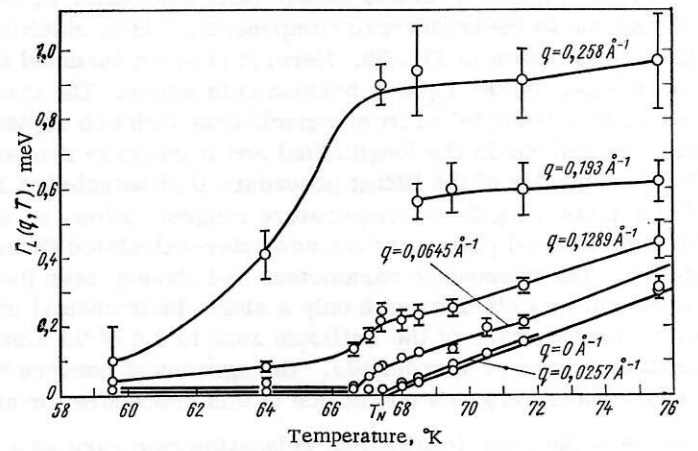

Fig. 9. Temperature dependence of the longitudinal diffusion width for different q.

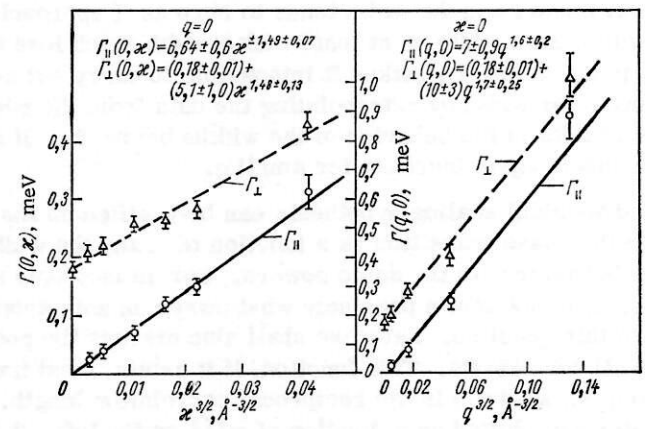

Fig. 10. Widths (at q = 0) as a function of $\varkappa$ when $T < T_N$ (on the left) and the widths at $T = T_N$ as a function of q. Both functions exhibit power-law behavior with power 3/2.

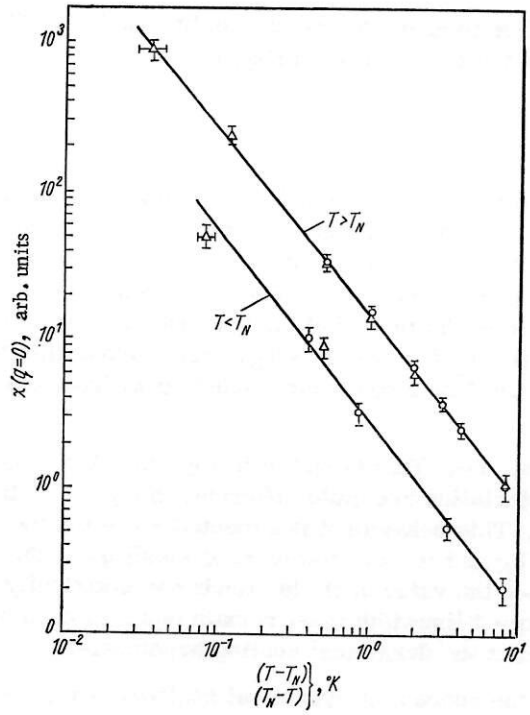

Fig. 11

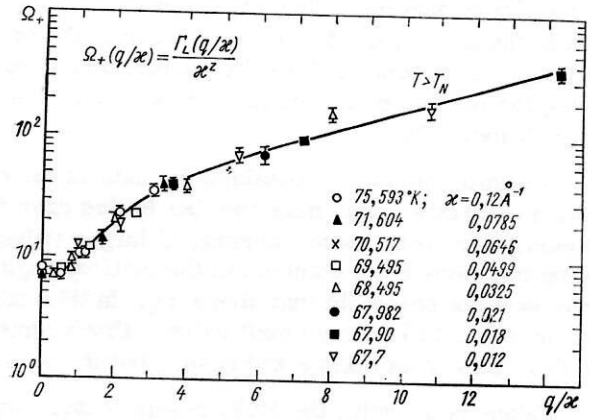

Fig. 12

Fig. 11. Behavior of the static magnetic susceptibility near the critical temperature: △) quasielastic scattering data; ○) inelastic neutron scattering data.

Fig. 12. Scaling function for longitudinal spin fluctuations at a temperature above the phase transition in MnF_2.

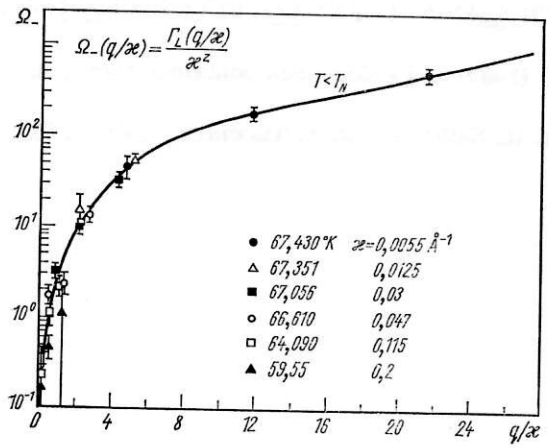

Fig. 13. Scaling function for longitudinal spin fluctuations at temperatures below the phase transition in MnF_2.

In the right-hand figure we have plotted the data relating to the dependences on $q^{3/2}$ for T_N and $\varkappa = 0$. In this case the fitted values of the exponents are 1.6 and 1.7, with a slightly greater error. The agreement between the two results is an excellent confirmation of the theory; moreover, within the experimental errors, we obtain the same 3/2 law as for an isotropic system.

Figure 11 shows the static susceptibility's behavior. The results of quasielastic measurements with a two-crystal spectrometer give us the correlation length and the susceptibility above T_N. Below T_N the presence of spin waves and the Bragg peak at $q = 0$ complicates the interpretation of the quasielastic measurements, but, to confirm the results obtained with the two-crystal spectrometer, we can use inelastic scattering. The figure shows that there is excellent agreement between the two methods.

The results for $T > T_N$ are shown in the top of the figure, while those for $T < T_N$ are at the bottom. The horizontal errors near T_N reflect the uncertainty of the value of the transition temperature. We can compare the ratio of χ above and below T_N by adjusting the data with the same exponent 4/3, which agrees with the experiment. We then obtain A_-/A_+ equal to 4.5 ± 0.2, which must be compared with 2 for molecular-field theory and 5 for the Ising model.

We now approach the question of a general scaling function to describe the data in the whole (q, T) plane. If such a function, let us call it Ω, exists, it must have the form shown in Fig. 12:

$$\Omega(q/\varkappa)=\frac{\Gamma_L(q/\varkappa)}{\varkappa z},$$

where z, as we have already established, is equal to 3/2. The figure shows how the experimental results appear when they are reduced to this form. In this figure, data for temperatures above the phase transition are given. They cover a wide range of q and temperatures. When q tends to zero, Ω takes on the value of the coefficient that describes the dependence of the q = 0 linewidth given above. When $\varkappa$ tends to zero, Ω tends to the asymptotic form that is valid in the critical region in the immediate neighborhood of T_N. There is no systematic temperature dependence apart from the decrease of $\varkappa$ as $T \to T_N$, which means that for given q the points are moved further outward. For example, the last three points include data from the interval 1° above T_N.

A similar picture is obtained for data in the region below T_N. This is shown in Fig. 13. A scaling function evidently exists here too, but in this case its characteristics are quite different. If $q/\varkappa > 4$, the two curves are very close, merging at larger values of $q/\varkappa$. This behavior was expected since the two scaling functions must coincide in the critical region at $T = T_N$ and $\varkappa = 0$. However, at small $q/\varkappa$, the curve does not resemble that above T_N. In this case, as $q \to 0$ the value of Ω also tends asymptotically to zero or at least to a very small value. This means that the q = 0 linewidth must remain equal to zero below T_N. This is an unexpected result, but it does not contradict the dynamical scaling hypothesis.

Taken as a whole, the MnF_2 results convincingly favor the concept of dynamical scaling. These results mean that, at least qualitatively, the second-order phase transition in a three-dimensional antiferromagnet is now understood. In the ferromagnetic metals Fe and Ni the experimental and theoretical problems are more complicated and the situation is less clear.

LITERATURE CITED

1. M. P. Schulhof, P. Heller, P. Nathans, and A. Linz, Phys. Rev., B1, 2304 (1970); Phys. Rev. Lett., 24, 1184 (1970).
2. M. J. Cooper and P. Nathans, Acta Cryst., 23, 357 (1967); A24, 481 (1968); A24, 619 (1968); A24, 624 (1968).
3. B. I. Halpern and P. C. Hohenberg, Phys. Rev., 177, 952 (1969) and references contained there, including references to work of Ferrell and co-workers.
4. H. Y. Lau, L. M. Corliss, A. Delapalme, J. M. Hastings, R. Nathans, and A. Tucciarone, Phys. Rev. Lett., 23, 1225 (1969); J. Appl. Phys., 41, 1384 (1970).